Dentomaxillofacial Radiology (2014) 43, 20130202

http://birpublications.org/dmfr

RESEARCH ARTICLE

Usefulness of 3T diffusion-weighted MRI for discrimination of reactive and metastatic cervical lymph nodes in patients with oral squamous cell carcinoma: a pilot study

[1,2]J Si, [2]S Huang, [3]H Shi, [2,4]Z Liu, [3]Q Hu, [3]G Wang, [1]G Shen and [2]D Zhang

[1]Department of Oral and Maxillofacial Surgery, Shanghai Ninth People's Hospital, Shanghai Jiao Tong University School of Medicine, Shanghai, China; [2]Department of Oral and Maxillofacial Surgery, Shandong Provincial Hospital affiliated to Shandong University, Jinan, China; [3]Shandong Provincial Medical Imaging Research Institute, Jinan, China; [4]Department of Head and Neck Oncology, West China College of Stomatology, Sichuan University, Chengdu, China

Objectives: To study the diagnostic accuracy of 3T diffusion-weighted MRI (DW-MRI) for the discrimination of reactive and metastatic cervical lymph nodes in patients with oral squamous cell carcinoma.

Methods: DW T_1 and T_2 weighted MRI was performed in 25 patients with biopsy-proved primary oral squamous cell carcinoma. The mean apparent diffusion coefficient (ADC) values of 30 histopathologically proved reactive lymph nodes and 21 histopathologically proved metastatic lymph nodes were compared using an unpaired *t*-test. A cut-off ADC value with optimal diagnostic sensitivity, specificity and area under the curve in discrimination of the two groups was determined using a receiver operating characteristic curve analysis.

Results: The mean ADC values of reactive lymph node and metastatic lymph node groups were $(1.037 \pm 0.149) \times 10^{-3}$ and $(0.702 \pm 0.197) \times 10^{-3}\,mm^2\,s^{-1}$, respectively. A statistically significant difference in ADC values of the two groups was certified ($p < 0.0001$). An optimal ADC threshold value of $0.887 \times 10^{-3}\,mm^2\,s^{-1}$ was suggested as the cut-off point, which resulted in 93.33% sensitivity, 80.95% specificity, 88.20% accuracy and area under curve of 0.887.

Conclusions: Our preliminary study indicates that the addition of 3T DW-MRI may be useful for discriminating between reactive lymph nodes and metastatic lymph nodes in patients with oral squamous cell carcinoma. However, larger studies are still required to validate our results and to standardize this imaging technique for daily clinical practice.
Dentomaxillofacial Radiology (2014) **43,** 20130202. doi: 10.1259/dmfr.20130202

Cite this article as: Si J, Huang S, Shi H, Liu Z, Hu Q, Wang G, et al. Usefulness of 3T diffusion-weighted MRI for discrimination of reactive and metastatic cervical lymph nodes in patients with oral squamous cell carcinoma: a pilot study. *Dentomaxillofac Radiol* 2014; **43:** 20130202.

Keywords: oral squamous cell carcinoma; cervical lymph node metastasis; diffusion-weighted magnetic resonance imaging; apparent diffusion coefficient

Introduction

Oral squamous cell carcinoma (OSCC), a malignant tumour from oral epithelial cells, is by far the most common malignant tumour in the oral cavity. Primary OSCC lesions can invade deeper layers below the epithelium and drain *via* the lymphatic route to regional lymph nodes in an early course.[1,2] Established clinical diagnostic and prognostic parameters of OSCC include the degree of histological differentiation, tumour size, invasion of the adjacent tissue and metastasis.[3] Although

Correspondence to: Dr Dongsheng Zhang. E-mail: ds63zhang@sdu.edu.cn

The first two authors (Jiawen Si and Shengyun Huang) contributed equally to this work.

Received 23 May 2013; revised 17 October 2013; accepted 7 January 2014

the localization and characterization of head and neck tumours have been well defined by CT and MRI, these conventional anatomy-based imaging methods still perform poorly in the assessment of lymph-node metastasis.[4,5] As proper assessment for the invasiveness and nodal metastasis of OSCC before operation has tremendous impact on patient management and prognosis, there is a clear need for new clinical indicators of diagnosis and advanced radiological techniques to improve the diagnostic accuracy for OSCC nodal metastasis.[2]

Diffusion-weighted MRI (DW-MRI), an unenhanced MRI technique previously applied in evaluating brain lesions, can reflect the level of random water molecular diffusion (Brownian motion) in tissue that are imaged and can be used to calculate the apparent diffusion coefficient (ADC) value of tissue in the region of interest.[6] As different types of tissue show distinct ADC values, the variations in ADC levels can be an important differential diagnostic criterion for malignancy and benign lesions.[6,7] Various researchers have applied DW-MRI in the detection of and characterization of tumours in different regions, such as the head and neck,[8–10] liver,[11,12] breast,[13,14] prostate,[15] bladder,[16] cervix,[17,18] ovary,[19] pancreas[20,21] and lungs.[22] In these studies, DW-MRI was found to have a high sensitivity and specificity in the detection of tumour mass. Previous studies have also investigated the significance of using DW-MRI in the evaluation of tumour response to (chemo)radiotherapy and the early distinction of therapy-induced tissue changes from local recurrence, as DW-MRI allows more precise differentiation between inflammatory tissue and tumour mass.[23,24] Besides, different studies have reported the ability of DW-MRI in the differentiation of benign and metastatic lymph nodes. Preliminary experiences indicated that DW-MRI may be helpful for nodal assessment in malignancies.[25–27]

To the best of our knowledge, although DW-MRI has been used to differentiate between malignant and benign lesions in the head and neck region on a large scale, there were few studies focusing on the ADC values for differential diagnosis of metastatic lymph nodes in OSCC. In this study, we report the ADC values derived from a 3T MRI scanner with dedicated 16-channel head and neck coils in a series of OSCC cases. Our aim was to investigate the diagnostic accuracy of DW-MRI with ADC calculation for the discrimination of reactive and metastatic lymph nodes in patients with OSCC.

Methods and materials

Patients

The study protocol was approved by our institutional ethics committee, and written informed consent was obtained from all patients prior to being included. From September 2010 to December 2012, 30 patients scheduled for surgical treatment (primary tumour resection and neck dissection) of biopsy-proved primary OSCC were prospectively enrolled. 5 out of the 30 patients were excluded, as they opted to receive non-surgical treatment. No patient had received treatment for head and neck cancer previously. All consecutive patients underwent routine head and neck 3T MRI (DWI included) at our institution within 5 days after biopsy and 1 week before surgery, regardless of the clinical tumour stage or nodal stage. A final diagnosis of reactive and metastatic lymph nodes was made by histopathological analysis of cervical lymph nodes derived from neck dissection according to standard histopathological procedures, and all slides were reviewed by one oral pathologist.

MRI protocol

All MRI examinations were performed with a 3 T MR scanner (Philips Achieva® 3 T; Royal Philips Electronics, Amsterdam, Netherlands) with a 16-channel head and neck coil. After a single-shot sagittal sequence was obtained to verify the position of the head and neck coil, all patients underwent axial T_1 and T_2 weighted turbo spin echo (TSE) and sagittal and coronal T_2 weighted TSE sequences using parameters shown in Table 1. The DW-MRI study was then processed by acquiring a single-shot echo-planar imaging sequence with three *b* values, using the technical parameters summarized in Table 2. To ascertain the correlation between conventional images and DW-MRI, the imaging of both conventional and DW-MRI ranged from the base of the skull to the level of the thoracic inlet, and all sequences were acquired using similar geometry.

Table 1 Scan sequences of T_1 and T_2 weighted turbo spin echo (TSE)

Parameters	*Sagittal* T_2 *weighted TSE*	*Axial* T_2 *weighted TSE*	*Coronal* T_2 *weighted TSE*	*Axial* T_1 *weighted TSE*
TR/TE	3000/90 ms	3000/90 ms	3000/90 ms	Shortest/10 ms
FOV (AP × RL × FH) (mm)	200 × 89 × 200	200 × 200 × 118	109 × 200 × 200	200 × 200 × 118
Voxel size (AP)/gap (mm)	0.75/1.0	0.75/0.5	0.75/1.0	0.75/0.5
Slice thickness (mm)	3	3	3	3
Recon voxel size (mm)	0.45	0.45	0.45	0.45
TSE factor	25	25	25	10
Flip angle	90	90	90	90
NSA	2	2	3	2
Total scan duration	2 min 6 s	2 min 32 s	3 min 9 s	4 min 38 s

AP, anteroposterior; FH, foot-to-head; FOV, field of view; NSA, number of signal averaged; RL, right-to-left; TE, echo time; TR, repetition time.

Table 2 Scan sequences of EPI-DWI

Parameters	*EPI-DWI*
TR/TE (ms)	3000/86 ms
FOV (AP × RL × FH) (mm)	200 × 200 × 118
Voxel size (AP × RL)(mm)	1.89/1.5
Slice thickness/gap (mm)	5.00/1.0
Recon voxel size	0.9
Fast imaging mode	EPI single-shot
EPI factor	55
Flip angle (degree)	90
NSA	3
Fat suppression	SPIR
Number of b factors	3
b-factor order	Ascending
Maximum b factor	800
Bandwidth (Hz)	26.0
ACQ voxel MPS (mm)	1.52/1.90/5.00
REC voxel MPS (mm)	0.89/0.89/5.00
Scan percentage (%)	79.70
Total scan duration	1 min 36 s

ACQ, acquisition; AP, anteroposterior; DWI, diffusion weighted imaging; EPI, echo-planar imaging; FH, foot-to-head; MPS, measurement phase slice; NSA, number of signal averaged; REC, reconstruction; RL, right-to-left; SPIR, selective partial inversion-recovery; TE, echo time; TR, repetition time.

Image analysis

For making the localization and analysis easier on an ADC map, lymph nodes with a maximum short axial diameter smaller than 1 cm were excluded from this study, with the exception of one metastatic lymph node (maximum short axial diameter: 0.8 cm), which could be detected and localized on the ADC map and was included in the study. All of the ADC measurements were separately made at an Advantage Windows Workstation version 4.1 (GE Medical Systems, Milwaukee, WI) by two radiologists with specific experience in head and neck imaging, who were blinded to all other clinical data and histopathological diagnosis. Regions of interest (ROIs) were drawn over the target lymph nodes on the ADC map with the aid of MR TSE images. In general, ROIs were placed carefully over the entire volume of the enlarged solid lymph nodes; in obvious necrotic lymph nodes, ROIs were placed on the solid tissue portions avoiding the necrotic components. The average ADC value of each lesion was calculated from three different ROIs within one lymph node.

Table 3 Patient characteristics

Patient no.	*Age (years)*	*Gender*	*Primary tumour location*	*Type of neck dissection*
1	72	M	Tongue	Selective
2	58	M	Cheek	Radical
3	57	F	Tongue	Radical
4	70	M	Tongue	Selective
5	73	M	Floor of mouth	Radical
6	66	M	Tongue	Radical
7	71	M	Cheek	Selective
8	65	F	Gingiva	Selective
9	59	F	Floor of mouth	Radical
10	55	M	Tongue	Radical
11	55	M	Cheek	Radical
12	81	M	Floor of mouth	Radical
13	52	F	Palate	Selective
14	72	F	Tongue	Radical
15	58	F	Tongue	Radical
16	62	M	Gingiva	Radical
17	64	M	Gingiva	Selective
18	60	M	Tongue	Selective
19	62	F	Cheek	Selective
20	64	M	Floor of mouth	Radical
21	59	M	Palate	Selective
22	62	M	Tongue	Radical
23	69	F	Floor of mouth	Radical
24	58	M	Cheek	Radical
25	59	F	Gingiva	Radical

F, female; M, male.

Table 4 Mean ADC values in metastatic and reactive cervical lymph nodes

Mean ADC of reactive LN ($\times 10^{-6}$ mm^2 s^{-1})	*Level of LN location*	*Mean ADC of metastatic LN ($\times 10^{-6}$ mm^2 s^{-1})*	*Level of LN location*
1178.0 ± 117.0	Level III	948.2 ± 90.4	Level V
908.5 ± 138.8	Level III	1076.6 ± 141.7	Level V
911.3 ± 54.9	Level I	935.3 ± 97.9	Level III
1074.1 ± 101.6	Level II	1126.8 ± 55.8	Level IV
1336.3 ± 82.7	Level II	569.2 ± 127.3	Level II
1351.6 ± 121.0	Level III	572.8 ± 111.7	Level II
923.5 ± 70.3	Level II	486.0 ± 96.0	Level II
895.0 ± 96.6	Level II	412.9 ± 129.8	Level I
1062.7 ± 126.4	Level III	504.6 ± 118.1	Level III
998.1 ± 113.3	Level I	517.0 ± 43.3	Level II
1091.2 ± 119.1	Level II	795.4 ± 120.6	Level I
1062.2 ± 114.4	Level III	624.1 ± 75.0	Level II
992.2 ± 105.0	Level II	640.3 ± 64.8	Level II
1041.7 ± 66.2	Level I	818.9 ± 65.0	Level I
912.5 ± 156.5	Level II	887.3 ± 64.8	Level III
1082.5 ± 88.0	Level II	684.5 ± 97.0	Level II
1073.7 ± 91.5	Level III	610.2 ± 91.7	Level II
1035.6 ± 40.5	Level I	716.9 ± 153.5	Level II
1014.6 ± 90.9	Level I	601.7 ± 134.2	Level III
1021.9 ± 43.7	Level II	645.3 ± 76.7	Level I
809.3 ± 71.5	Level II	572.3 ± 156.5	Level II
877.3 ± 133.0	Level II		
924.4 ± 55.4	Level II		
1370.4 ± 46.4	Level I		
1003.3 ± 79.0	Level III		
940.6 ± 103.1	Level II		
959.4 ± 57.7	Level II		
947.8 ± 64.1	Level II		
1366.5 ± 106.9	Level III		
932.3 ± 59.4	Level I		

ADC, apparent diffusion coefficient; LN, lymph node.

Pathological–radiological correlation

Surgical procedures were performed by the same experienced oral and maxillofacial surgeon who was blinded to the number and localization of cervical lymph nodes detected by MRI. After surgery, the fresh dissected neck specimens were carefully delineated and tagged by the surgeon according to the American Academy of Otolaryngology–Head and Neck Surgery classification system. Then, all lymph nodes were progressively identified, separated, fixed, sectioned and subsequently examined microscopically by one specialized oral pathologist who was also blinded to the radiological findings. By recording the combination of the maximum short axial diameter and the exact location of each enlarged lymph

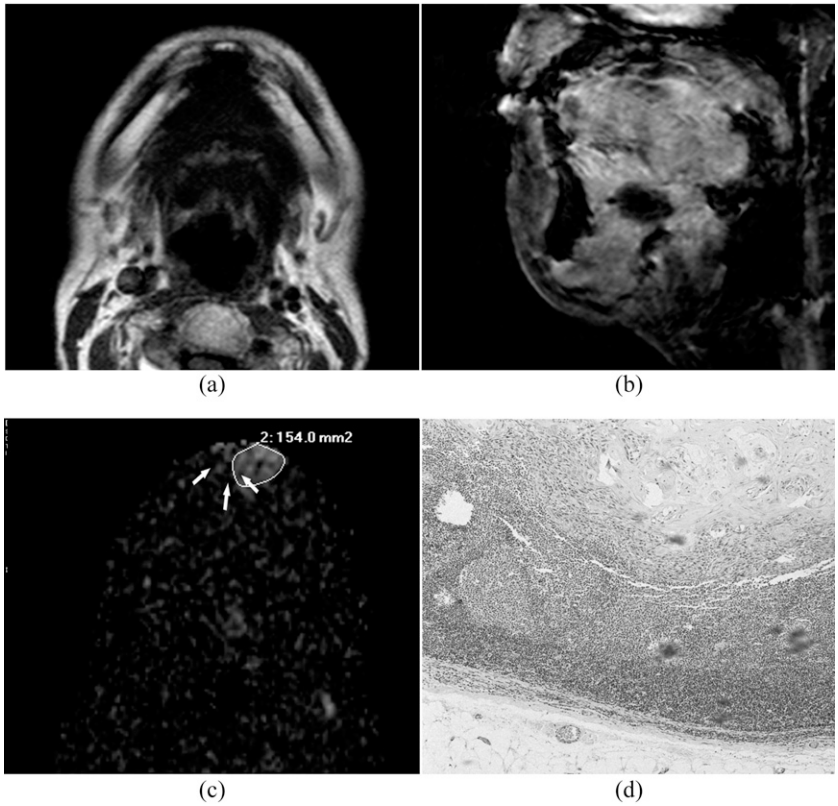

Figure 1 Images of a 37-year-old patient with well-differentiated squamous cell carcinoma of gingival: (a, b) transverse T_1 weighted MR image and sagittal fat-suppressed T_2 weighted MR image show no hyperintensity of submental lymph nodes. (c) A heterogeneous enhancement (white arrows) in submental region is observed on the diffusion-weighted image at b = 800 s mm^{-12} which results in a low apparent diffusion coefficient value of $(0.795.4 \pm 0.121) \times 10^{-3}$ mm^2 s^{-1}. (d) Histopathological examination (haematoxylin and eosin stain; original magnification, ×40) shows that tumour cells are deposited within the metastatic lymph node, and enlarged nuclei, high nucleus–cytoplasm ratio and pathological mitotic figures are observed.

node correlated to adjacent anatomical structures, such as the submandibular gland, sternocleidomastoid muscle, and jugular vein, it was possible to perform a topographic correlation for each enlarged lymph node between the pathological results and the MR images.[5,27,28] If the pathologist detected more lymph nodes than the radiologist observed in MRI, it was feasible to choose the largest lymph node as the one observed in images.[8] The histopathological results were used as the reference standard, which was prospectively compared with the DW-MRI values of each enlarged lymph node.

Statistical analysis

Histopathological results in terms of the presence or the absence of lymph node metastasis were used as reference standard; lymph nodes (maximum short axial diameter >1.5 cm) without OSCC metastasis were included as the reactive lymph node group. The mean ADC values between the reactive lymph node group and the metastatic lymph node group were compared using an unpaired Student's *t*-test. To evaluate the diagnostic performance of ADC measurements in differentiating metastatic lymph nodes from reactive lymph nodes, a receiver operating characteristic (ROC) curve analysis was performed. An optimal threshold value was calculated as the cut-off point that best discriminated between the two groups in terms of maximum sensitivity and minimum number of false-positive results. $p < 0.05$ was considered statistically significant. Numeric data were reported as means ± standard deviations. Statistical analysis was performed using SPSS® v. 17.0 (SPSS Inc., Chicago, IL) and MedCalc software (MedCalc Software, Ostend, Belgium).

Results

The mean age of the 25 patients with OSCC was 63.32 years (range, 52–81 years; 9 females and 16 males) (Table 3). In total, 897 lymph nodes were dissected during histopathological examination, and MR images revealed 346 of these nodes, among which 30 reactive lymph nodes and 21 metastatic lymph nodes were identified. Most identified lymph nodes were situated at Level I ($n = 11$), Level II ($n = 25$), or Level III ($n = 12$). Only three nodes were detected at Level IV ($n = 1$) or Level V ($n = 2$) (Table 4).

In the assessment of DW-MRI images of the 51 identified lymph nodes, the metastatic lymph nodes

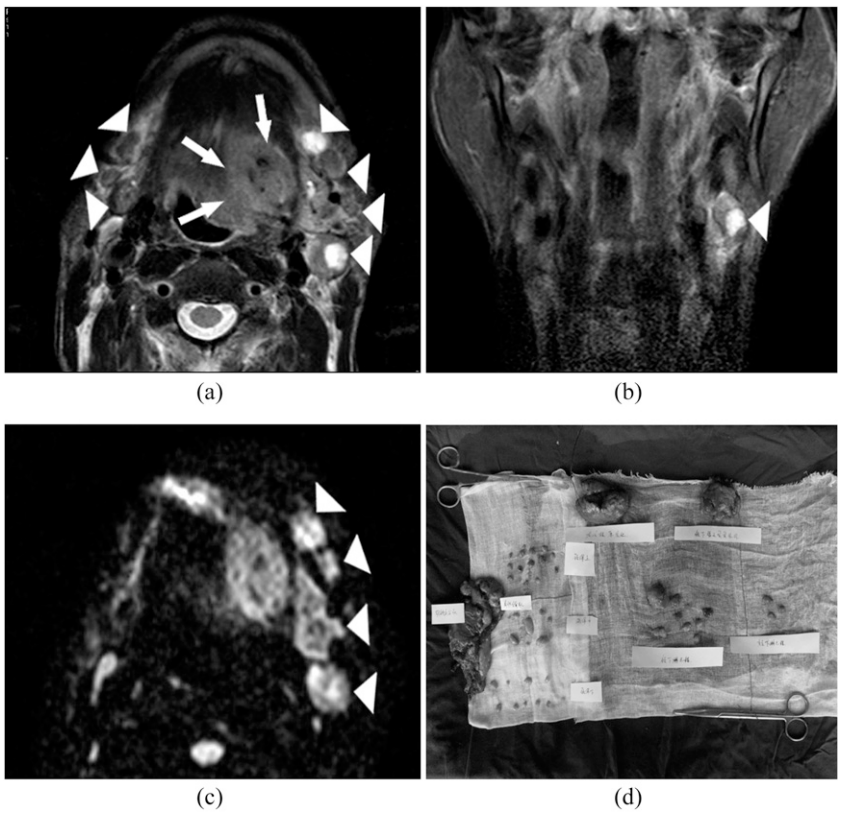

Figure 2 (a, b) Images of a 54-year-old patient presenting with a biopsy-proven squamous cell carcinoma in the left-side of the tongue. The patient presents with a left-sided tongue tumour (white arrows). Several enlarged lymph nodes are visible on both sides (white arrowheads) of T_2 weighted images. (c) Four lymph nodes are visible in the left neck (white arrowheads) with hyperintensity on the b = 800 diffusion-weighted image. The corresponding apparent diffusion coefficient values of left-sided metastatic lymph nodes are $(0.685 \pm 0.097) \times 10^{-3}$ mm^2 s^{-1}, $(0.61 \pm 0.092) \times 10^{-3}$ mm^2 s^{-1}, $(0.717 \pm 0.154) \times 10^{-3}$ mm^2 s^{-1}, respectively; while the apparent diffusion coefficient value of one left-sided reactive lymph nodes is $(0.809 \pm 0.072) \times 10^{-3}$ mm^2 s^{-1}. (d) After surgery, the fresh dissected neck specimens are carefully delineated and tagged by the surgeon. Histopathological analysis of cervical lymph nodes with haematoxylin and eosin staining confirms metastatic deposits in three left-sided lymph nodes.

show significant enhancement compared with reactive lymph nodes in DW images (Figures 1–3). The mean ADC values in the reactive and metastatic lymph nodes were $(1.037 \pm 0.149) \times 10^{-3}$ and $(0.702 \pm 0.197) \times 10^{-3}$ mm^2 s^{-1}, respectively ($p < 0.0001$). A statistically significant difference in ADC values of the two groups was certified. An optimal threshold value of 0.887×10^{-3} mm^2 s^{-1} was suggested as the cut-off point in ROC analysis of the 2 groups, which resulted in 17 true-positive, 2 false-positive, 28 true-negative and 4 false-negative findings, yielding 93.33% sensitivity, 80.95% specificity, 88.20% accuracy and area under the ROC curve reaching 0.887, with 95% confidence interval (CI) from 0.767 to 0.959 (Figure 4). Besides, we also compared the average ADC values of all lymph nodes in the selective and radical neck dissection group. However, no significant difference was found between the two groups (data are not shown).

Discussion

Although significant differences in ADC values between benign and malignant lesions have been clinically validated in several independent studies, the biophysical basis for these lower ADC values in malignant tumours are still poorly understood. According to previous data in the literature, potential reasons for the decreased ADC values within malignancies were probably related to a combination of higher cellularity, cellular polymorphism, diminished extracellular space and keratinization, all contributing to reduced motion of water.[6,29] Thus, malignant lesions, such as metastatic lymph nodes, tend to show low ADC values; non-tumour tissue changes with low cellularity, such as inflammation and fibrosis, are expected to show strong contrast with tumour masses.[7,27,30] However, this correlation between ADC values and tissue characterization may not be applicable to all tumours, such as adenocarcinomas, lymphomas and neoplastic necrosis.[6,31,32] As tumours of different pathological types may demonstrate a wide range of ADC values along with their variable microstructural features, our study is unique in that it mainly focused on the evaluation of DW-MRI in routine clinical cervical nodal assessment of patients with histopathology-proved OSCC.

To our knowledge, using DW-MRI to characterize head and neck tumours and to differentiate malignant from benign lesions has been investigated in several

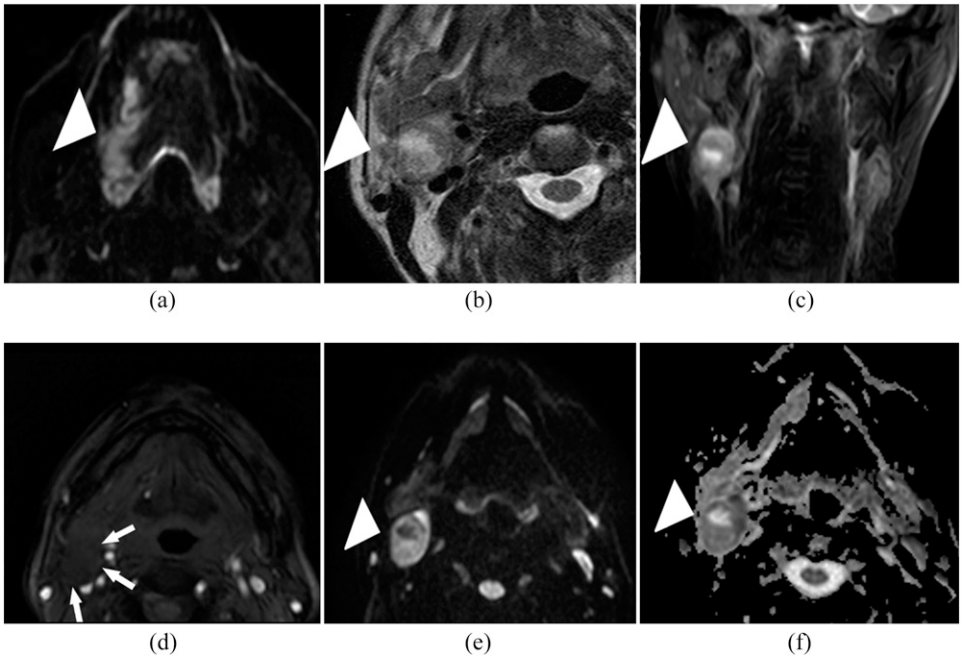

Figure 3 Images of a 50-year-old male patient with a biopsy-proven squamous cell carcinoma in the tongue. (a) The patient with a biopsy-proven squamous cell carcinoma in the tongue on the right side (white arrowhead). (b, c) The transverse and coronal T_2 weighted image shows a right-sided enlarged lymph node with central necrosis (white arrowhead) in Level II. (d) Gadolinium-enhanced T_1 weighted image shows no enhancement within the enlarged lymph node (white arrows). (e) This lymph node is easily recognized on the diffusion-weighted image at b = 800 (white arrowhead) in which histopathological examination confirms metastatic deposits. (f) The corresponding area (white arrowhead) on the apparent diffusion coefficient map shows a calculated apparent diffusion coefficient of $(0.64 \pm 0.065) \times 10^{-3}\,mm^2\,s^{-1}$.

former studies.[8–10,30] In line with these prior studies focusing on the diagnostic accuracy of DW-MRI in head and neck malignancies, the results of our study demonstrate a significant difference of ADC values between reactive and metastatic lymph nodes in 25 OSCC cases. Although there was a tiny overlap of ADC values between reactive and metastatic lymph nodes, the 25th and 75th centile region did not show any overlap. The result of ROC analysis suggested that 0.887×10^{-3} mm^2 s^{-1} may prove to be the threshold ADC value for differentiation between reactive and metastatic cervical lymph nodes with 93.33% sensitivity, 80.95% specificity, and 88.20% accuracy (Figure 4). This indicates that DW-MRI may be applied in differential diagnosis of cervical metastasis from reactive lymph nodes in patients with OSCC.

Interestingly, only few reports have demonstrated the usefulness of DW-MRI in characterizing regional lymph node metastasis. Published data have shown that ADC measurement on DW-MRI may be helpful in discriminating metastatic from benign lymph nodes. In one early study performed in patients with cervical lymph node lesions of different pathological types by Sumi et al,[33] significantly higher ADC values were observed in metastatic lymph nodes than in benign lymph nodes. This finding suggests that DW-MRI may help to discriminate benign from metastatic lymph nodes in the neck. However, contrary to the findings of Sumi et al, remarkable lower ADC values have been reported in several later studies. In one study by Abdel Razek et al[32] the mean ADC values of both metastatic lymph nodes and lymphomas were $(1.09 \pm 0.11) \times 10^{-3}$ and $(0.97 \pm 0.27) \times 10^{-3}\,mm^2\,s^{-1}$, respectively—significantly lower than those of benign lymph nodes. Another study focusing on ADC values between benign and malignant head and neck lesions at 3T MRI demonstrated a statistically significant difference between the mean ADC values in the benign and malignant lesions [$(1.505 \pm 0.487) \times 10^{-3}$ and $(1.071 \pm 0.293) \times 10^{-3}\,mm^2\,s^{-1}$, respectively], and ADC threshold values of $1.3 \times 10^{-3}\,mm^2\,s^{-1}$ may be the threshold value for the differentiation between benign and malignant head and neck lesions.[8] Moreover, preliminary results have also suggested the possibility for the detection of subcentimetric nodal metastases in head and neck.[5,34] However, partial volume effect when drawing ROIs on the DW-MRI maps around these small lymph nodes may lead to significant false-positive results.[28] Besides, inclusion of smaller nodes may lead to higher potential bias in image interpretation and, most importantly, pathological–radiological correlation. Therefore, we excluded the lymph nodes with a maximum short axial diameter <1 cm.

Our results, although based on a small population of patients, are largely consistent with previous reports without taking varying ADC values into consideration. The differences of ADC threshold values among these studies probably come forth not only owing to different pathologies, techniques and platforms that were used in

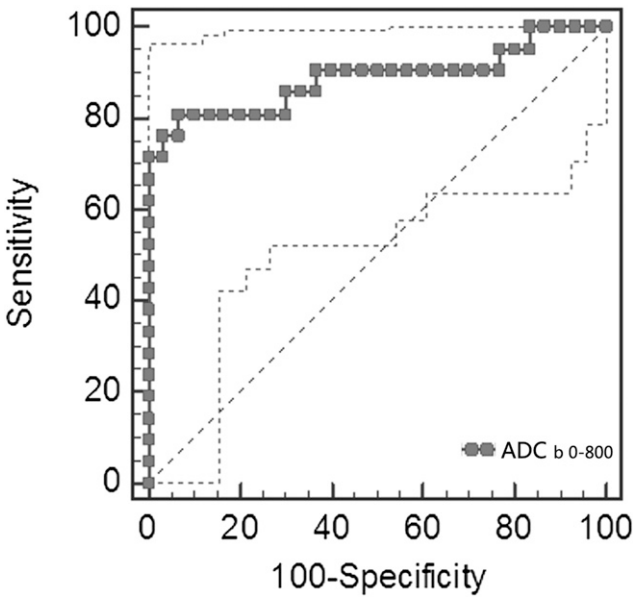

Figure 4 An optimal threshold value of $0.887 \times 10^{-3}\,mm^2\,s^{-1}$ is suggested as the cut-off point, which results in 93.33% sensitivity, 80.95% specificity and 88.20% accuracy; area under the receiver operating characteristic curve reaches as high as 0.887, with 95% confidence interval from 0.767 to 0.959 ($p < 0.0001$). ADC, apparent diffusion coefficient.

MRI but also the ROI selection of the examined lymph nodes, especially in metastatic ones, as intranodal necrosis or liquefaction tend to occur in large metastatic lymph nodes, which can result in notably higher ADC values and an underestimation of lesion extent.[5,30,31] To avoid the effect of intranodal necrosis, we kept ROIs on the solid portions of target lymph nodes, away from the necrotic components. It is worth noting that we found one pathologically proved metastatic lymph node with large intranodal necrosis in MR-TSE images, while no obvious signal enhancement was observed in DW-MRI (Figure 5).

According to the comparisons in previously reported literatures and our own experience, better sensitivities and specificities were obtained using DW-MRI than CT or conventional MRI in staging cervical lymph node metastasis.[5,33] Although we did not assess the effect of combining DW imaging with TSE MRI on diagnostic accuracy, it is judicious to surmise that the high sensitivity of conventional MR sequences for necrosis or liquefaction may help to prevent necrosis-induced false-negative rate of DW-MRI.[7,35] Thus, we prefer synthetic application of DW-MRI and conventional MR sequences in the pre-treatment nodal staging of OSCC, other than single application of ADC values for diagnosis and nodal assessment. Furthermore, combining DW-MRI with conventional MRI was suggested as a better approach to precisely localize the lesion and to obtain reliable ADC values.[9,16,25]

Nevertheless, some limitations of this study have to be addressed. Firstly, potential bias in image interpretation cannot be entirely excluded, because either image reading or ROI selection was clinically made by radiologists, through which ADC values is not measured in a standardized way of generating data. However, as reported earlier in the literature,[5,8,28] we utilized double reading to minimize the effects. Also, owing to the retrospective nature of our study, the possibility of a selection bias cannot be excluded. Secondly, we did not study the correlation between different technical settings and ADC quantification, even though it has a major influence on ADC calculation.[9,29,33] Therefore, agreement on protocol and parameter standardization should be a major issue for the near future. Thirdly, this described DW-MRI technique is not a panacea for all limits in OSCC metastasis diagnosis. Since the performance of DW-MRI in the detection of subcentimetric nodal metastases in the head and neck region was not evaluated in most studies, it is not yet possible to single out ADC values to perform diagnosis and nodal staging. Further studies should focus on the comparison or integration of DW-MRI with other advanced imaging

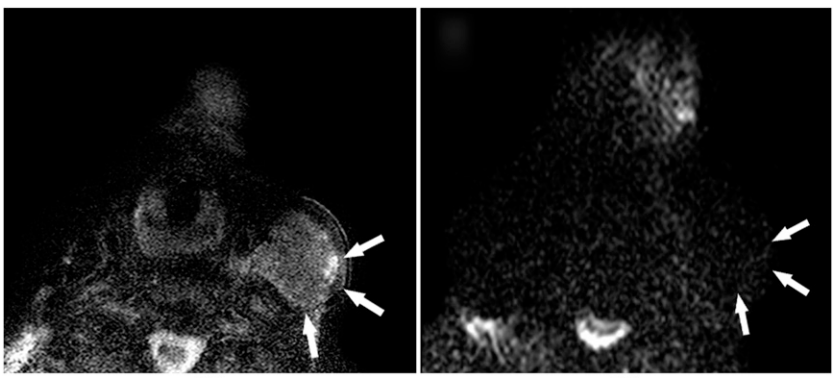

Figure 5 Images of an 81-year-old male patient with a biopsy-proven squamous cell carcinoma in the floor of the mouth. (a) transverse T_2 weighted image demonstrates an enlarged lymph node with heterogeneous hyperintensity and necrotic areas on Level IV (white arrows). (b) The large histopathological proven metastatic lymph node (white arrows) is barely visible on the b = 800 image. The apparent diffusion coefficient value of the assessed nodal portion is $(1.077 \pm 0.142) \times 10^{-3}\,mm^2\,s^{-1}$, probably owing to the large necrotic areas within the tumour.

techniques in pretreatment assessment of OSCC. Fourthly, ADC measurements were obtained by calculating three ROIs in one target lymph node, which may not be fully representative for the overall sample profile. However, this approach was chosen for time-saving and better feasibility in daily clinical practice. Finally, we have not performed any correlation between the ADC values and long-term outcome, and further study with larger numbers of cases will be required to validate the long-term prognosis.

Conclusion

In conclusion, we have demonstrated that ADC measurement from the DW-MRI is a useful quantitative parameter in the differential diagnosis of cervical metastasis in patients with OSCC. The significantly lower ADC values of metastatic cervical lymph nodes (solid portions) compared with reactive cervical lymph nodes therefore confirms the complementary value of DW-MRI for nodal characterization. Besides, an ADC cut-off point of $0.887 \times 10^{-3}\,mm^2\,s^{-1}$ as the threshold value for differential diagnosis of OSCC metastatic lymph nodes is preliminarily obtained by ROC analysis. The available evidence indicates that the addition of DW-MRI may be useful in routine clinical diagnosis of cervical lymph node metastasis in patients with OSCC, although larger prospective studies are required to validate our results and to focus on the standardization of this imaging technique.

References

1. Kumaran PS, Thangaswamy SV, Navaneetham A. The need for early detection of neck nodal metastasis in squamous cell carcinoma of oral cavity. *J Pharm Bioallied Sci* 2012; **4**: S341–3. doi: 10.4103/0975-7406.100300
2. Leusink FK, van Es RJ, de Bree R, Baatenburg de Jong RJ, van Hooff SR, Holstege FC, et al. Novel diagnostic modalities for assessment of the clinically node-negative neck in oral squamous-cell carcinoma. *Lancet Oncol* 2012; **13**: e554–61. doi: 10.1016/S1470-2045(12)70395-9
3. Massano J, Regateiro FS, Januario G, Ferreira A. Oral squamous cell carcinoma: review of prognostic and predictive factors. *Oral Surg Oral Med Oral Pathol Oral Radiol Endod* 2006; **102**: 67–76. doi: 10.1016/j.tripleo.2005.07.038
4. Castelijns JA, van den Brekel MW. Imaging of lymphadenopathy in the neck. *Eur Radiol* 2002; **12**: 727–38. doi: 10.1007/s003300101102
5. Vandecaveye V, De Keyzer F, Vander Poorten V, Dirix P, Verbeken E, Nuyts S, et al. Head and neck squamous cell carcinoma: value of diffusion-weighted MR imaging for nodal staging. *Radiology* 2009; **251**: 134–46. doi: 10.1148/radiol.2511080128
6. Padhani AR, Liu G, Koh DM, Chenevert TL, Thoeny HC, Takahara T, et al. Diffusion-weighted magnetic resonance imaging as a cancer biomarker: consensus and recommendations. *Neoplasia* 2009; **11**: 102–25.
7. Thoeny HC, De Keyzer F, King AD. Diffusion-weighted MR imaging in the head and neck. *Radiology* 2012; **263**: 19–32. doi: 10.1148/radiol.11101821
8. Srinivasan A, Dvorak R, Perni K, Rohrer S, Mukherji SK. Differentiation of benign and malignant pathology in the head and neck using 3T apparent diffusion coefficient values: early experience. *AJNR Am J Neuroradiol* 2008; **29**: 40–4. doi: 10.3174/ajnr.A0743
9. Verhappen MH, Pouwels PJ, Ljumanovic R, van der Putten L, Knol DL, De Bree R, et al. Diffusion-weighted MR imaging in head and neck cancer: comparison between half-fourier acquired single-shot turbo spin-echo and EPI techniques. *AJNR Am J Neuroradiol* 2012; **33**: 1239–46. doi: 10.3174/ajnr.A2949
10. King AD, Mo FK, Yu KH, Yeung DK, Zhou H, Bhatia KS, et al. Squamous cell carcinoma of the head and neck: diffusion-weighted MR imaging for prediction and monitoring of treatment response. *Eur Radiol* 2010; **20**: 2213–20. doi: 10.1007/s00330-010-1769-8
11. Heijmen L, Ter Voert EE, Nagtegaal ID, Span P, Bussink J, Punt CJ, et al. Diffusion-weighted MR imaging in liver metastases of colorectal cancer: reproducibility and biological validation. *Eur Radiol* 2013; **23**: 748–56. doi: 10.1007/s00330-012-2654-4
12. Le Moigne F, Durieux M, Bancel B, Boublay N, Boussel L, Ducerf C, et al. Impact of diffusion-weighted MR imaging on the characterization of small hepatocellular carcinoma in the cirrhotic liver. *Magn Reson Imaging* 2012; **30**: 656–65. doi: 10.1016/j.mri.2012.01.002
13. Ochi M, Kuroiwa T, Sunami S, Murakami J, Miyahara S, Nagaie T, et al. Diffusion-weighted imaging (b value = 1500 s/mm(2)) is useful to decrease false-positive breast cancer cases due to fibrocystic changes. *Breast Cancer* 2013; **20**: 137–44.
14. Martincich L, Deantoni V, Bertotto I, Redana S, Kubatzki F, Sarotto I, et al. Correlations between diffusion-weighted imaging and breast cancer biomarkers. *Eur Radiol* 2012; **22**: 1519–28. doi: 10.1007/s00330-012-2403-8
15. Doo KW, Sung DJ, Park BJ, Kim MJ, Cho SB, Oh YW, et al. Detectability of low and intermediate or high risk prostate cancer with combined T2-weighted and diffusion-weighted MRI. *Eur Radiol* 2012; **22**: 1812–19. doi: 10.1007/s00330-012-2430-5
16. Avcu S, Koseoglu MN, Ceylan K, Bulut MD, Unal O. The value of diffusion-weighted MRI in the diagnosis of malignant and benign urinary bladder lesions. *Br J Radiol* 2011; **84**: 875–82. doi: 10.1259/bjr/30591350
17. Cao K, Gao M, Sun YS, Li YL, Sun Y, Gao YN, et al. Apparent diffusion coefficient of diffusion weighted MRI in endometrial carcinoma-Relationship with local invasiveness. *Eur J Radiol* 2012; **81**: 1926–30. doi: 10.1016/j.ejrad.2011.04.019
18. Seo JM, Kim CK, Choi D, Kwan Park B. Endometrial cancer: utility of diffusion-weighted magnetic resonance imaging with background body signal suppression at 3T. *J Magn Reson Imaging* 2013; **37**: 1151–9. doi: 10.1002/jmri.23900
19. Li W, Chu C, Cui Y, Zhang P, Zhu M. Diffusion-weighted MRI: a useful technique to discriminate benign versus malignant ovarian surface epithelial tumors with solid and cystic components. *Abdom Imaging* 2012; **37**: 897–903.
20. Jang KM, Kim SH, Kim YK, Park MJ, Lee MH, Hwang J, et al. Imaging features of small (</= 3 cm) pancreatic solid tumors on gadoxetic-acid-enhanced MR imaging and diffusion-weighted imaging: an initial experience. *Magn Reson Imaging* 2012; **30**: 916–25. doi: 10.1016/j.mri.2012.02.017
21. Niwa T, Ueno M, Ohkawa S, Yoshida T, Doiuchi T, Ito K, et al. Advanced pancreatic cancer: the use of the apparent diffusion coefficient to predict response to chemotherapy. *Br J Radiol* 2009; **82**: 28–34. doi: 10.1259/bjr/43911400
22. Gumustas S, Inan N, Akansel G, Ciftci E, Demirci A, Ozkara SK. Differentiation of malignant and benign lung lesions with diffusion-weighted MR imaging. *Radiol Oncol* 2012; **46**: 106–13. doi: 10.2478/v10019-012-0021-3
23. Belli P, Costantini M, Ierardi C, Bufi E, Amato D, Mule A, et al. Diffusion-weighted imaging in evaluating the response to neoadjuvant breast cancer treatment. *Breast J* 2011; **17**: 610–19. doi: 10.1111/j.1524-4741.2011.01160.x
24. Kim HS, Kim CK, Park BK, Huh SJ, Kim B. Evaluation of therapeutic response to concurrent chemoradiotherapy in patients with

cervical cancer using diffusion-weighted MR imaging. *J Magn Reson Imaging* 2013; **37**: 187–93. doi: 10.1002/jmri.23804
25. Klerkx WM, Veldhuis WB, Spijkerboer AM, van den Bosch MA, Mali WP, Heintz AP, et al. The value of 3.0Tesla diffusion-weighted MRI for pelvic nodal staging in patients with early stage cervical cancer. *Eur J Cancer* 2012; **48**: 3414–21. doi: 10.1016/j.ejca.2012.06.022
26. Pauls S, Schmidt SA, Juchems MS, Klass O, Luster M, Reske SN, et al. Diffusion-weighted MR imaging in comparison to integrated [^{18}F]-FDG PET/CT for N-staging in patients with lung cancer. *Eur J Radiol* 2012; **81**: 178–82. doi: 10.1016/j.ejrad.2010.09.001
27. Fornasa F, Nesoti MV, Bovo C, Bonavina MG. Diffusion-weighted magnetic resonance imaging in the characterization of axillary lymph nodes in patients with breast cancer. *J Magn Reson Imaging* 2012; **36**: 858–64. doi: 10.1002/jmri.23706
28. De Bondt RB, Hoeberigs MC, Nelemans PJ, Deserno WM, Peutz-Kootstra C, Kremer B, et al. Diagnostic accuracy and additional value of diffusion-weighted imaging for discrimination of malignant cervical lymph nodes in head and neck squamous cell carcinoma. *Neuroradiology* 2009; **51**: 183–92.
29. Charles-Edwards EM, deSouza NM. Diffusion-weighted magnetic resonance imaging and its application to cancer. *Cancer Imaging* 2006; **6**: 135–43. doi: 10.1102/1470-7330.2006.0021
30. Ichikawa Y, Sumi M, Eida S, Takagi Y, Tashiro S, Hotokezaka Y, et al. Apparent diffusion coefficient characterization of fluid areas in cystic and abscess lesions of the neck. *Oral Radiology* 2012; **28**: 62–9.
31. Kato H, Kanematsu M, Kato Z, Teramoto T, Mizuta K, Aoki M, et al. Necrotic cervical nodes: usefulness of diffusion-weighted MR imaging in the differentiation of suppurative lymphadenitis from malignancy. *Eur J Radiol* 2013; **82**: e28–35. doi: 10.1016/j.ejrad.2012.08.014
32. Abdel Razek AA, Soliman NY, Elkhamary S, Alsharaway MK, Tawfik A. Role of diffusion-weighted MR imaging in cervical lymphadenopathy. *Eur Radiol* 2006; **16**: 1468–77. doi: 10.1007/s00330-005-0133-x
33. Sumi M, Sakihama N, Sumi T, Morikawa M, Uetani M, Kabasawa H, et al. Discrimination of metastatic cervical lymph nodes with diffusion-weighted MR imaging in patients with head and neck cancer. *AJNR Am J Neuroradiol* 2003; **24**: 1627–34.
34. Kitajima K, Yamasaki E, Kaji Y, Murakami K, Sugimura K. Comparison of DWI and PET/CT in evaluation of lymph node metastasis in uterine cancer. *World J Radiol* 2012; **4**: 207–14. doi: 10.4329/wjr.v4.i5.207
35. King AD, Tse GM, Ahuja AT, Yuen EH, Vlantis AC, To EW, et al. Necrosis in metastatic neck nodes: diagnostic accuracy of CT, MR imaging, and US. *Radiology* 2004; **230**: 720–6. doi: 10.1148/radiol.2303030157